VERSITA

OPTO-ELECTRONICS REVIEW **18**(3), 318–327

DOI: 10.2478/s11772-010-1022-y

Uncooled MWIR and LWIR photodetectors in Poland

J. Piotrowski[1], J. Pawluczyk[1], A. Piotrowski[1], W. Gawron[*2], M. Romanis[1], and K. Kłos[1]

[1]VIGO System S.A., 129/133 Poznańska Str., 05-850 Ożarów Maz., Poland
[2]Institute of Applied Physics, Military University of Technology, 2 Kaliskiego Str., 00-908 Warsaw, Poland

The history, status, and recent progress in the middle and long wavelength $Hg_{1-x}Cd_xTe$ infrared detectors operating at near room temperatures are reviewed. Thermal generation of charge carriers in narrow gap semiconductor is a major limitation or sensitivity. Cooling is a straightforward way to suppress thermal generation of charge carriers and reduce related noise. However, at the same time, cooling requirements make infrared systems bulky, heavy, and inconvenient in use. A number of concepts to improve performance of photodetectors operating at near room temperatures have been proposed and implemented. Recent considerations of the fundamental detector mechanisms suggest that near perfect detection can be achieved without the need for cryogenic cooling. This paper, to a large degree, is based on the research, development, and commercialization of uncooled HgCdTe detectors in Poland. The devices have been based on 3D-variable band gap and doping level structures that integrate optical, detection and electric functions in a monolithic chip. The device architecture is optimized for the best compromise between requirements of high quantum efficiency, efficient and fast collection of photogenerated charge carriers, minimized thermal generation, reduced parasitic impedances, wide linear range, wide acceptance angles and other device features. Recent refinements in the devices design and technology have lead to sensitivities close to the background radiation noise limit, extension of useful spectral range to > 16 μm wavelength and picosecond range response times. The devices have found numerous applications in various optoelectronic systems. Among them there are fast scan FTIR spectrometers developed under MEMFIS project.

Keywords: infrared photodetectors, uncooled detection, HgCdTe, graded gap structures.

1. HgCdTe photodetectors in Poland

In 1959, British scientists [1] discovered photoelectrical properties of $Hg_{1-x}Cd_xTe$ alloy that became the most important material for MWIR and LWIR photodetectors. Polish efforts in the field started immediately [2–4].

1.1. The Institute of Physics Polish Academy of Sciences

The HgCdTe research began in 1960 at the Institutes of Physics of Warsaw University and Polish Academy of Sciences (IFPAN), Warsaw. Bridgman technique with sealed thick wall quartz ampoules was used to grow material suitable for research and experimental devices. The explosions caused by the high mercury pressure were quite frequent that time, resulting in a few series accidents. The grown material was used for optical and galvanomagnetic studies. The studies were aimed at determination of energy band structure of the material. The $Hg_{1-x}Cd_xTe$ studies were for a long time the main topics of numerous meetings on solid state physics and electronics in Poland. The studies were important contribution to the understanding of fundamental properties of the material.

Simple photoconductive, photoelectromagnetic, and photovoltaic devices based on the bulk MCT crystals were demonstrated already in 1963 [5]. Interesting, the first photovoltaic devices were based on *n*-on-*p* junctions that were formed at perimeter of MCT ingots during cool down period. Later, IFPAN scientists concentrated their efforts on diluted magnetic semiconductors such as $Hg_{1-x}Mn_xTe$, less useful for infrared photodetectors.

1.2. The Military University of Technology

In 1968, device-oriented research started at the Military University of Technology (MUT), Warsaw (see Ref. 6 and related papers therein). Initially, modification of the isothermal vapour phase epitaxy (ISOVPE) discovered by Cohen-Solal *et al.* [7] in France, was applied. The original process relies on near-equilibrium isothermal evaporation of HgTe upon a thick CdTe substrate [Fig. 1(a)]. Interdiffusion of the grown layer with the substrate material yields variable gap structures.

In the Polish modification [8] [Fig. 1(b)], the hybryde substrates with thin CdTe layers were used rather than the bulk CdTe. The layers had been deposited by vacuum evaporation on low-cost and readily available substrates such as mica, silicon, sapphire and other. Limited amount of HgTe was then deposited by ISOVPE and the process was carried out up to complete homogenization. As the result, extremely uniform epitaxial layers were grown.

*e-mail: wgawron@wat.edu.pl

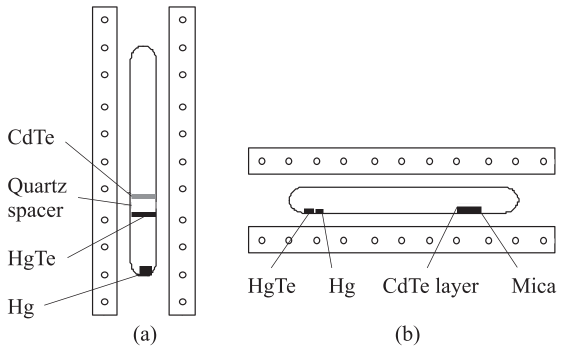

Fig. 1. ISOVPE growth in sealed ampoules: (a) original ISOVPE technique and (b) Polish modification.

The layers were used as the basis for fabrication of photoconductive, photoelectromagnetic, and photovoltaic detectors operating in the MWIR and LWIR range at near room temperature [6,8–11]. The first long wavelength (10.6 μm) detectors operating at high temperatures (HOT detectors) were demonstrated already in 1972 [6,9] and used in laser fusion research.

Bulk growth had also been tried. For this purpose, a modification of the quench-anneal technique was developed in which the quenched ingot was annealed in temperature gradient perpendicular to the axis of the ingot [12–14]. Uniform and high quality $Hg_{1-x}Cd_xTe$ and $Hg_{1-x}Zn_xTe$ crystals have been grown. They were used both for studies of the material properties and for practical IR devices. The other subjects of the research were *p*-to-*n* conversion with ion implantation, ion milling, and anodic oxidation of $Hg_{1-x}Cd_xTe$ and other Hg-based materials [15,16].

The need for complex heterostructures for high quality infrared devices, especially those operating at near room temperature devices, has been recognized. Initially, buried *N-p* junction photodiodes grown by ISOVPE were used to reduce dark current in photodiodes [17]. Hot wall epitaxy [18] and the LPE [19] growth from Te-rich solution has been also tried.

The MUT group is also known for studies of fundamental problems of the infrared detection [20], detector modelling [21], and, especially, for numerous Rogalski's books and excellent review papers on infrared detectors [22–29].

1.3. Other

Significant efforts on $Hg_{1-x}Cd_xTe$ detectors were at Wrocław Technical University. The ISOVPE growth was extensively studied [30–35]. High quality photovoltaic devices with *n*-on-*p* junction formed by Hg in-diffusion had been demonstrated. This group was near to commercialization of the liquid nitrogen cooled photovoltaic devices, but eventually failed to achieve the goal. The main problem was a low producibility of the sealed ampoule technique and limitation of conventional ISOVPE growth – the lack of extrinsic doping and heterojunction passivation.

The $Hg_{1-x}Cd_xTe$ related research has been carried out also at the Institute of Electron Technology, the Institute of Vacuum Technology, Rzeszów University of Technology, the Military Institute of Armament Technology, and many other institutions. Extensive studies of photoelectromagnetic effect in $Hg_{1-x}Cd_xTe$ have been carried out at Silesian Technical University [36].

2. Commercialization of infrared photodetector

The commercialization of the infrared detectors in Poland started in the early 1980's, initially at the Institute of Plasma Physics and Laser Microfusion and then at a spin-off SME VIGO System S.A., Warsaw. The niche market strategy has been pursued with a goal of the versatile production of the uncooled infrared photodetectors optimized for operation at any wavelength within the short-, middle-, and long-wavelength range of infrared spectrum. Significant development efforts were necessary.

2.1. Heterostructure photodetector concept

In the early 1990's, the VIGO System team recognized fundamental limitations to performance of the infrared detectors imposed by unavoidable physic of the thermal generation and ways to perfect detection without cooling was proposed and implemented [37–41]. The general expression for maximum detectivity of any type detector was derived [41]

$$D^* = 0.64k\lambda\left(\frac{A_o}{A_e}\right)^{1/2}\left(\frac{\alpha}{G}\right)^{1/2}.$$

The ratio of absorption coefficient to the bulk thermal generation, rate α/G, is the basic figure of merit of any semiconductor material for infrared photodetector. A_o/A_e is the ratio of the optical to physical area of the detector. The coefficient k reflects enhanced absorption measures, $k = 2^{1/2}$ and 1 for single and double pass of radiation through the absorber. Further, gain ($k > 1$) can be obtained with the use of optical resonant cavity.

The last expression assumes absorber as the only source of thermal generation of charge carriers. In practice, thermal generation may occur at surfaces, contacts, interfaces and other regions of an infrared detector.

To achieve the ultimate performance in practice, Vigo developed a concept of a photodetector as a monolithic heterostructure chip (Fig. 2) that integrates optical, detection and electronic functions, important for device operation [38–44], concentration of radiation, enhanced absorption, efficient and fast collection, suppression of thermal generation, minimized parasitic impedances and internal photoelectric gain. Typically, the device consists of following parts:

- monolithic optical immersion microlenses as optical concentrators formed from the substrates of epitaxial layers. One order gain in detectivity and two-order gains in RC time constant-limited speed of response have been obtained with GaAs hyperhemispherical immersion lenses. The single microlenses of 0.5 to 10 mm dia were

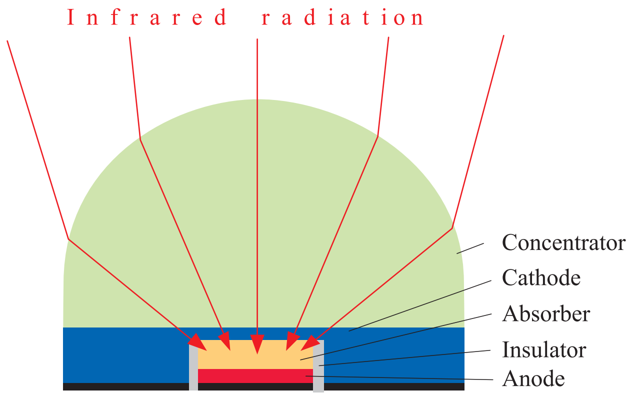

Fig. 2. Schematic illustration of 3D heterostructure photodetector.

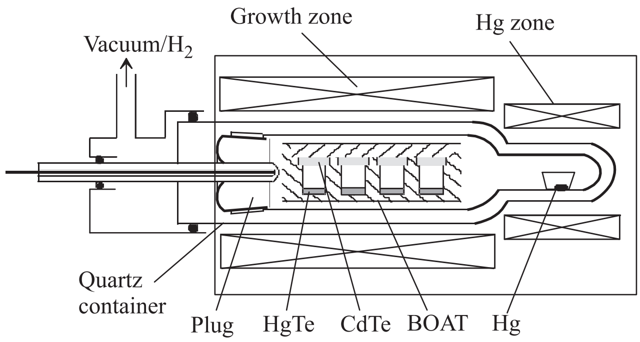

Fig. 3. Isothermal vapour phase growth reactor.

prepared by conventional optical machining while smaller lenses and 2D arrays have been prepared with photolithography assisted etching,

- infrared absorber with band gap, composition and thickness optimized for the best compromise between requirements of efficient use of IR radiation and low thermal generation,
- wide gap and heavily doped contact regions to minimize parasitic impedances,
- graded gap interfaces to suppress thermal generation,
- retroreflector to enhance absorption of IR radiation and shield against background optical generation.

The heterostructures have been designed to obtain a low finesse optical resonance due to reflections at the substrate-heterostructure interfaces, internal interfaces, and the heterostructure top surface.

During the last two decades, various infrared devices based on the concept have been developed including photoconductive, photoelectromagnetic, magnetoconcentration, Dember and photovoltaic detectors [38,40–46].

2.2. Open tube ISOVPE growth

Despite of many years of R&D, no economically efficient HgCdTe growth technology was available in Poland when Vigo System was established. The solution was a unique production-type atmospheric pressure system was developed in cooperation with Djuric's group from Belgrade University [47,48] and has been used for commercial fabrication of HgCdTe photodetectors for many years. The epitaxial system shown in Fig. 3 allows for several large area layers grown in one growth run. Mercury loss was reduced to few milligrams per growth by the use of quartz container with a conical quartz plug. The system has two independently controlled temperature zones, the mercury zone (20–400°C) and the growth zone (~500°C). Layers with thicknesses from < 1 μm to > 1 mm and any compositions could be obtained, in dependence on growth conditions. Typically, it took less than two hours to grow a ~10-μm thick device heterostructure. For a good lateral uniformity (x < 0.005), variation of the temperature in the growth zone should be less than 0.3 K. In-depth band gap profiles have been shaped in controlled way by variations of growth conditions and subsequent post-growth annealing. The necessary growth conditions can be theoretically predicted using computer simulation of ISOVPE based on generalized model of the process [49]. As-grown epilayers exhibit a significant grading (Fig. 4) but heat treatment at ~400°C in increased mercury vapour pressure results in near-uniform composition in the most part of the layer (2/3 of total thickness). To reduce concentration of vacancies, the process is completed with programmed cooling down the growth and mercury zones. Low 10^{15} cm^{-3} electron concentration has been typically obtained. The relatively high carrier concentrations probably results from impurities either in the substrates, source materials, gases, or contaminants on the substrate surface.

Initially, the doping level was controlled by heat treatment in mercury vapour to establish concentration determined by the difference between concentration of native acceptors and residual donor impurities. Later, extrinsic doping with Au and As during growth has been used. Some layers were *ex-situ* doped by In or Au diffusion and ion milling.

In contrast to the low temperature epitaxial techniques (LPE, MOCVD and MBE), ISOVPE yields smooth surface morphology, independently on substrate orientations. Therefore, low cost large grain polycrystalline CdTe or CdZnTe substrates have been used. The other choice is composite substrates, GaAs, sapphire, silicon with predeposited CdTe layer. The HgTe sources are polycrystalline wafers used for many growth runs (> 15). In general, the technique is characterized by low consumption of starting materials – mercury, tellurium and cadmium, much less than for any other $Hg_{1-x}Cd_xTe$ growth technique. Several methods have been used to modify in-depth and lateral composition profiles [50].

Negative epitaxy. This is reversed ISOVPE process based on near-equilibrium evaporation of HgTe from $Hg_{1-x}Cd_xTe$ in H_2/Hg atmosphere at relatively low temperatures (300–400°C) in the same ISOVPE growth reactor. The technique has been extensively used to widen band gap of 0.5–2 μm surface region for passivation purposes (Fig. 4). The negative epitaxy combined with As doping from gas phase was also used for formation of heavily doped P^+ contacts.

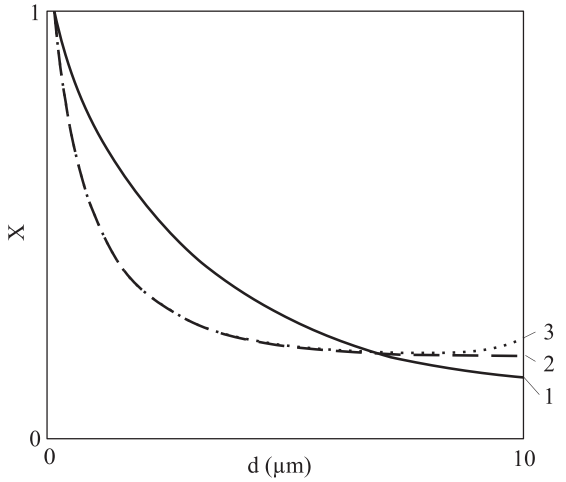

Fig. 4. Compositional profiles of epilayers obtained by ISOVPE: 1 – as grown, 2 – after heat treatment, and 3 – after negative epitaxy.

Selective epitaxy. Selective epitaxy can be achieved by ISOVPE growth on openings in SiO_x layers deposited on $Hg_{1-x}Cd_xTe$ (Fig. 5). SiO_x layer prevents epitaxy on covered substrate since interdiffusion between substrate and growing layer is blocked.

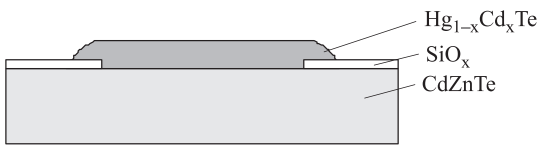

Fig. 5. Schematic cross-section of epilayer obtained by selective ISOVPE.

Epitaxy on profiled CdTe substrates. In this method, the ISOVPE growth is carried out onto CdTe substrate with etched off deeps or tranches. Next, the substrate is mechano-chemically polished for flat surface. The process has been used for fabrication of photodiodes burried in CdTe substrates (Fig. 6).

Post growth deposition of CdTe or CdTe/ZnS. CdTe/ZnS layers were used in some devices for surface passivation in addition to widening of band gap of near surface region with negative epitaxy.

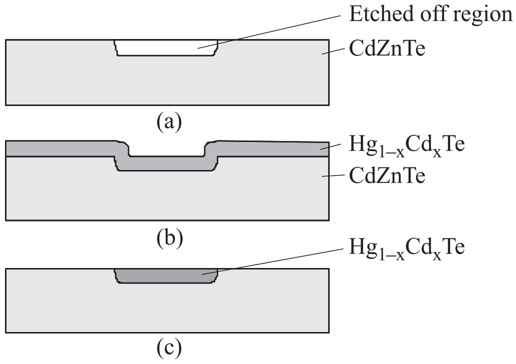

Fig. 6. Epitaxy on profiled CdTe substrates: (a) etched off pockets in CdTe substrate (b) ISOVPE grown HgCdTe layer, and (c) burried HgCdTe structure.

2.3. MOCVD growth

In 2003, VIGO System and MUT established common MOCVD laboratory with AXT 200 II-VI dedicated system. The main motivation was fabrication of more complex HgCdTe heterostructures and use of large substrates. Successful growth of multilayer heterostructures has been demonstrated on CdTe, GaAs and other substrates. The present status is described in papers [51–54].

Hydrogen is used as a carrier gas. Dimethylcadmium (DMCd) and diisopropyltelluride (DIPTe) precursors are held in temperature-stabilized baths. Ethyl iodine (EI) is used as a donor and tris-dimethyloaminoarsenic (TDMAAs) as acceptor dopant source. DMCd and EI are delivered through the upper channel of growth reactor while DIPTe and TDMAAs are delivered through the lower channel over the quartz container where elementary mercury is held. The substrate and the mercury vapour source are heated with halogen radiators.

IMP mode is used for controllable growth of heterostructures with complex composition and doping profiles. Numerous improvements have been introduced such as:

- online control of precursor transport with IR gas analyzer and laser reflectometer,
- stoichiometry adjustment during growth with non-equilibrium treatment with cadmium vapour,
- solutions for programmed growth of graded gap and doping structures,
- final growth stage procedures to obtain low vacancy material and without any post-growth anneal,
- various measures for reduced precursors consumption and shorter growth time,
- MOCVD has been also used for overgrowth of wide gap HgCdTe structures for passivation and other purposes. A low temperature (~300°C) growth procedure has been developed to prevent modification of a composition profile [55].

2.4. Detector fabrication

Figure 7 shows flow chart of manufacturing photodetectors. The fabrication procedure is similar for photoconductive, photoelectromagnetic, and photovoltaic devices.

The fabrication starts from characterization of the epitaxial structures and typically involves optical inspection, on-wafer Hall effect and SIMS measurements, transmittance, reflectance and photoresponse spectroscopy.

Active elements are delineated with photolithography--assisted ion milling and wet chemical etching. Contact metallization is deposited by sputtering of Cr/Au using lift--off technique. The wafers are diced into individual chips and immersion lens prepared from the substrates of the epilayer. The chips with immersion lenses are flip-chip bonded to an Au/Cr pattern on sapphire or directly, on ceramic cold fingers of Peltier coolers.

The last stage of detector preparation is detector sealing in various packages, backfilled with Xe or Kr/Xe mixture.

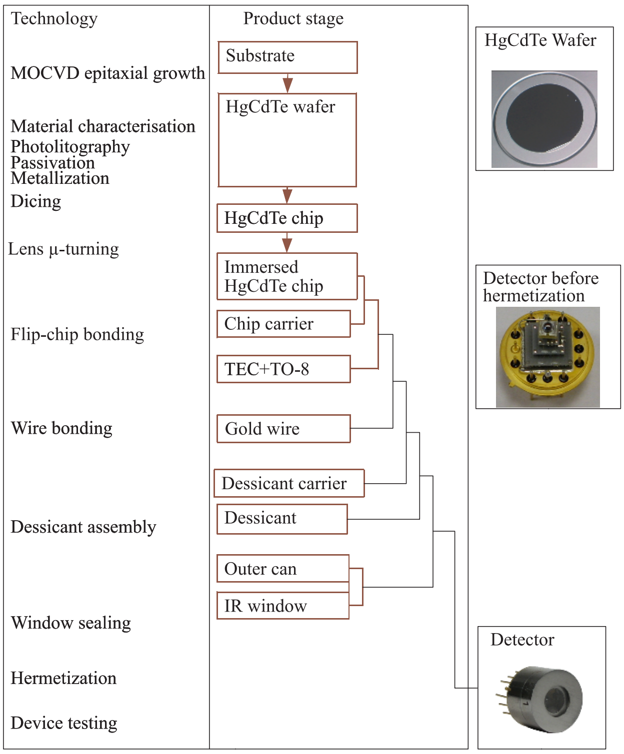

Fig. 7. Manufacturing process flow.

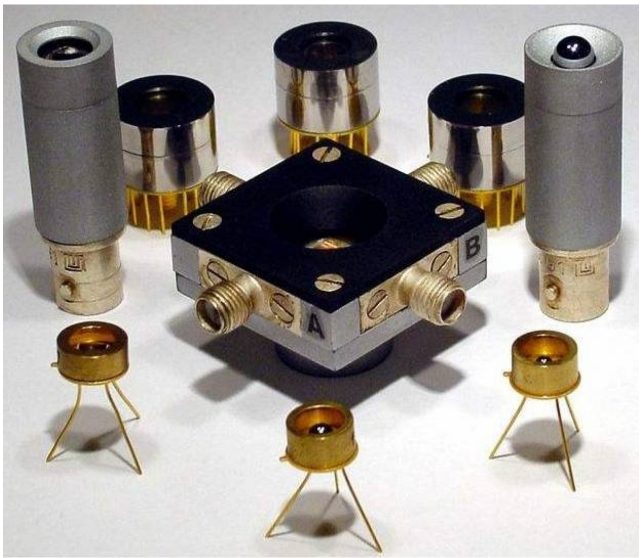

Fig. 8. Packages of uncooled and Peltier cooled detectors.

Uncoated or AR coated ZnSe is typically as IR transmitting windows. Various absorbers of water vapours, CO_2 and absorber are used to prevent water condensation and improve detector stability.

The housed devices have been typically integrated with associated electronics (readout transimpedance preamlifiers that provide also optimized bias to detectors, Peltier cooler controllers and A/D converters) in detection modules. This makes them convenient to use and immune to EMI and prevents electrostatic or transient overbias.

2.5. Devices

At present, VIGO System S.A. offers photoconductive, photoelectromagnetic, and photovoltaic devices (Fig. 8) optimized for any wavelength in the LWIR, MWIR, and SWIR range of infrared spectrum [56]. The longest usable wavelengths are 11 µm, 13 µm, and 16 µm for uncooled, 2- and 3-stage Peltier coolers, respectively. The formats are single elements with sizes from few µm to a few mm, linear arrays up to 120 elements, small 2D arrays.

Without optical immersion photovoltaic detectors are sub-BLIP devices with performance limited by thermal generation. Well designed optically immersed MWIR devices approach BLIP limit when cooled with 2-stage Peltier coolers. Situation is less favourable for > 8 µm LWIR photovoltaic detectors. Despite of all improvements (advanced architecture, optical immersion, Peltier cooling) they show detectivities below the BLIP limit by more than order of magnitude. Typically, the devices are used at zero or near zero bias. The attempts to use Auger suppressed non-equilibrium devices were not very successful due to a large 1/*f* noise extending to 100 MHz both in extracted photodiodes and magnetoconcentration devices [45].

The devices are characterized by a very fast response. The uncooled 10-µm photodetectors show 1 ns or less response time, determined by a short recombination time. More slow are < 10 µm PC devices, especially thermoelectrically cooled. Their speed of response could be improved with heavier doping than required for optimized performance or using sweep out of minority carriers. Much faster are photoelectromagnetic devices in which time constant is much shorter than the bulk recombination time due to fast diffusion of minority carriers to a high recombination velocity surface.

Lastly, the photovoltaic devices have been optimized for fast operation. The RC time constant was shorten by reduced physical area of devices with optical immersion and improved architecture to widen space charge region. The series resistance was minimized to few ohms or less using heavily doped N^+ for base regions of the mesa structures and elimination of parasitic impedances. Picosecond range response time was measured in many devices using various sources of short pulses of IR radiation such as free electron and quantum cascade lasers, synchrotron sources and parametric converters [57,58].

The uncooled or Peltier cooled photodetectors have found numerous applications [45,46]. They are used mostly for industrial and scientific applications. The examples are pyrometry, thermal imaging, conventional, laser and FTIR spectroscopy, gas analyzers, plasma physics, laser metrology, laser technology, laser microfusion experiments, free space optical communication, various CO_2 and numerous quantum cascade laser based systems. Their military applications are laser rangefinders, alerters, lidars, guidance, tracking and many other applications.

3. LWIR photodetectors for FTIR applications

The typical requirements for FTIR spectrometer detector are specific, high sensitivity within a wide spectral range (2 to 16 μm), relatively low electric signal frequencies (400 Hz to ~100 kHz), good linearity and stability. The thermal radiation sources used in FTIRs produce intensive photon flux in the spectral range of 3–5 μm that may saturate detector response and generate radiative noise. In contrast, the flux is weak at the wavelength < 2.5 μm and > 7 μm so, high sensitivity is required.

Pyroelectric detectors have important advantages for conventional slow scan FTIR systems. They operate at ambient temperature, have unselective spectral response and increase performance with decreasing signal frequencies corresponding to long wavelength. Unfortunately, their performance is quite poor at frequencies exceeding 100 kHz, as required for short wavelength or/and new portable fast scan FTIRs. An example is MEMS interferometer being developed at present under the MEMFIS project [59] that requires optimized operation for electrical frequencies 100 kHz to 2 MHz.

We describe here development of Peltier cooled photoconductors and photodiodes dedicated to fast scan FTIR spectrophotometers with spectral response extended to 16 μm.

3.1. Photoconductive detectors

Picture shows shematic cross-section of two types of photoconductive detectors (Fig. 9). The first one is a modification of PCI-2TE detector used for long time for FTIR spectrophotometers with *p*-type absorbers of x = 0.175 nominal composition that should ensure operation up to 16 μm at a temperature of 190 K, achievable with miniature 4-stage Peltier coolers. Characterization of the device revealed "shorter" response at 193 K than expected, peak response at ~10 μm, 50% cutoff at 12 μm, 7.5% response at 14 μm followed by a soft Urbach tail at longer wavelengths. This was caused by larger than expected absorber gap as confirmed by the Hall effect and SIMS measurements. Since the band gap of low x HgCdTe is critically dependent on composition, even minor growth faults result in significant deviations of spectral response.

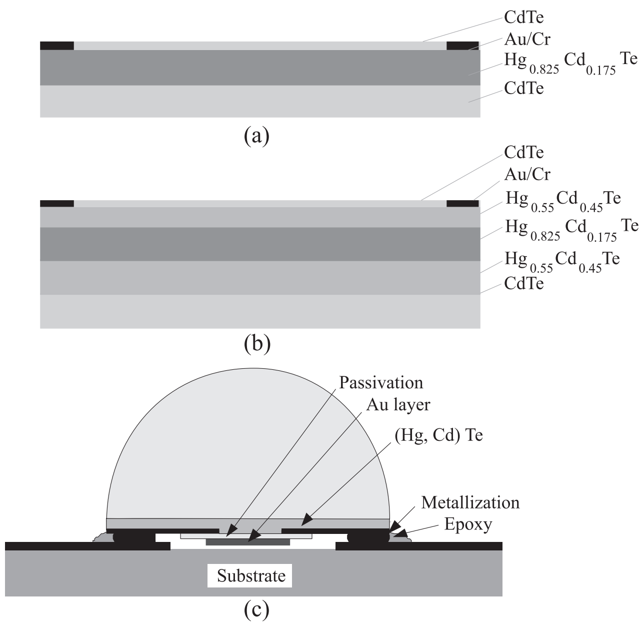

Fig. 9. Schematic structures of photoconductive detectors with single absorber (a), with double absorber (b), and chip of opically immersed photoconductive detector mounted on a substrate (c).

The practical devices have shown 1/*f* noise with ~10 kHz knee followed by frequency independent noise at higher frequencies. The detectivities of optically immersed devices at frequencies 100 kHz–2 MHz were 1.4×10^9, 4.4×10^9 and 0.56×10^9 cmHz$^{1/2}$/W at 2.5 μm, 11 μm and 14 μm, respectively, close to the MEMFIS requirements. The measurements were made with detectors integrated with preamplifiers, so preamplifier noise was included.

The linearity of response was measured using 1300 K blackbody focused at detector plane. The device has shown linear response up to ~1.2 mW/mm^2 optical power densities.

The two-absorber solution [Fig. 8(b)] has been applied in improved devices for independent performance optimization at the short < 3-μm and long < 14-μm spectral range in purpose to compensate decreasing spectral photon flux of the thermal sources. More thick surface passivation layers should provide better passivation. As follows from calculations, the fundamental performance limit due to the Auger generation and recombination is ~1×10^9 cmHz$^{1/2}$/W at 14 μm for non-immersed detector operating at 190 K, while optically immersed devices should exceed. With the use of exceed the MEMFIS requirements improved linearity range is expected because the intensive 3–5 μm radiation will be absorbed in the long wavelength absorber characterized by a short recombination time. The structures with modified composition and doping profiles have been already grown and devices are processed at present.

3.2. Photodiodes

Photodiodes are the most promising devices for FTIR applications offering better performance and wider linearity range [44]. The advantages have been clearly demonstrated for < 5-μm photodiodes operating with simple one or two--stage Peltier coolers that exhibit near ideal performance with noise limited by quantum noise of incoming radiation [55]. Development of > 11-μm wavelength photodiode operating at near room temperatures presents a significant challenge, however. The devices are usually limited by large bulk, tunnel and depletion dark currents, parasitic impedances and poor match to preamplifiers. They also show significant 1/*f* noise in the required frequency range. The limitations are of technological rather than fundamental nature [60,61] and can be overcome with device design, growth, and processing refinements.

3.2.1. Numerical simulation and optimization

The photodiode (Fig. 10) is essentially an $N^{+}pP^{+}$ structure with graded interfaces. We have considered structures with following layers:

- uniform N^{+} layer acting as electron contact and playing also a role of the short-wavelength (~2.5 µm) cut-on window,
- lightly doped 4- to 7-µm thick absorber with compositions of 0.17 to 0.19, *p*-type doped in the 10^{15}–10^{17} cm^{-3} range,
- graded gap and doping level interface between N^{+} layer and absorber, *p*-type doped within 10^{15}–10^{17} cm^{-3} range,
- graded gap and doping level *p*-type interface between absorber and P^{+} hole contact,
- heavily doped (~10^{17} cm^{-3}) P^{+} hole contact,
- ~10^{17} cm^{-3} p^{+} graded gap interface between absorber and contact metallization to reduce contact resistance.

The calculations were carried out using the Apsys package [62]. Several optimized architectures were selected for zero and reverse bias operation.

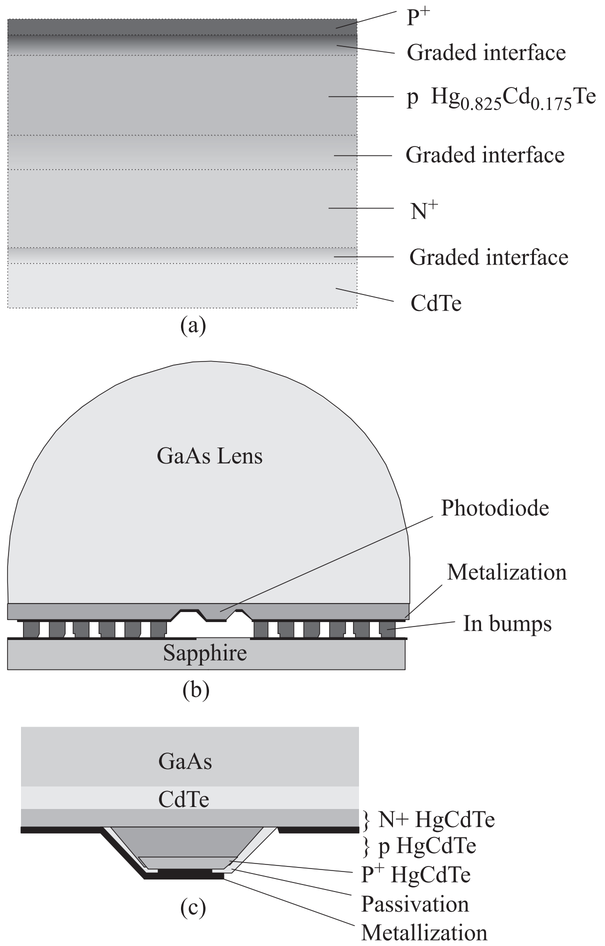

Fig. 10. (a) Schematic structure of ~14-µm photodiode, (b) flip-chip mounted detector, and (c) enlarged cross-section of the mesa device. The mesa top metallization serves as a contact and backside mirror providing double pass of the weakly absorbed long wavelength radiation.

Zero bias operation. The optimized devices for operation at zero bias require absorber of ~10^{16} cm^{-3} p-type doping and narrow lightly doped absorber interfaces. The devices show good collection efficiency but current responsivity are reduced by a factor ~2 due a low zero bias resistance (<10 Ω), comparable with the series resistance. The low photodiode resistance presests a significant challenge for coupling to electronics increasing the resulting noise.

Reverse bias operation. Simulations show that optimized architecture of the photodiodes (Fig. 11) should ensure low dark current, large differential resistance, high quantum efficiency and fast collection of photogenerated carriers. The selected architecture results in flat conductive and valence bands within the absorber region (Fig. 12). Since electric fields is located only in wide gap and lightly doped parts of interfaces, the device should be free from tunnel currents.

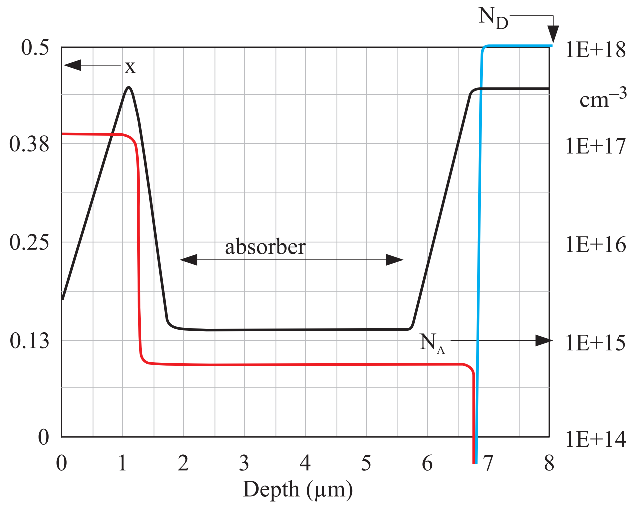

Fig. 11. Composition and doping profiles of 14-µm photodiode structure optimized for 0.5 V reverse bias at 190 K. The structures are characterized by linear composition grading between absorber and contacts for minority and majority carriers.

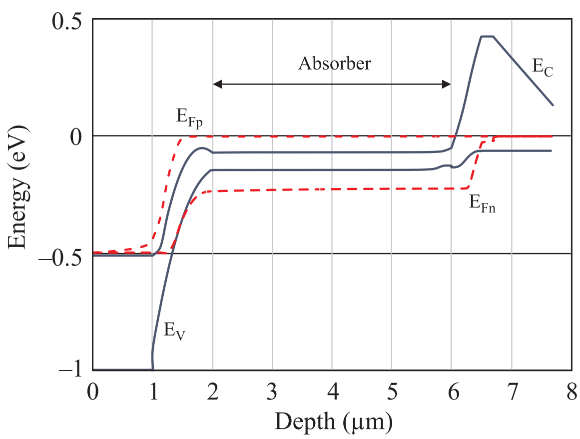

Fig. 12. Band diagram of a reverse biased structure.

The calculated I-V plot (Fig. 13) is typical for extracted photodiodes [63] and consists of three regions:

- low voltages 0 to V_{max} with dark current increasing with voltage to I_{max},
- negative resistance region with dark current decreasing from I_{max} to I_{sat}. An interesting feature is photoelectric gain larger than unity. The gain decreases to unity at $V \sim V_{sat}$,
- saturated dark current I_{sat} region for $V >> V_{sat}$. The current is due to Auger 7 generation in the absorber.

The I_{max}/I_{sat} ratio depends on device architecture and may be quite large (~100). The operations at voltages equal or larger than V_{max} are of special interest for detection due to a low dark current and related shot noise. The other advantages are good current responsivity, fast response, good linearity and large differential resistance providing good match to electronics.

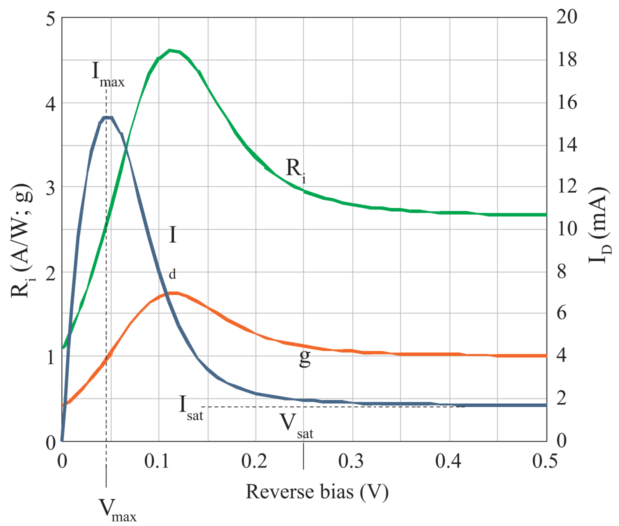

Fig. 13. Dark current per 0.1×0.1 mm^2 detector physical area, current responsivity, and photoelectrical gain *vs*. reverse voltage.

The results of numerical calculations are very promising. The saturated dark current density is quite low (~0.25 A/cm^2), a factor of ~2 greater than the dark current generated by the 300 K background radiation and significantly less than current generated by the FTIR signal radiation. The calculations do not take into account other than Auger dark currents, such as the radiative generation due to thermal radiation of the detector surrounding, tunnel and Shockley-Read dark currents. The last mechanism seems to be the most significant and will exceed the Auger 7 current by a large factor.

3.2.2. Practical photodiodes

Prototype ~14 μm photodiodes were fabricated and characterized by measurements of dark currents, spectral current responsivity, photoelectric gain and spectral detectivity. The measured I-V plot (Fig. 14) show a narrow saturation range. The dynamic resistance in the saturation range 0.08–0.13 V is >100 Ω. Tunnel-like currents are observed at larger voltages.

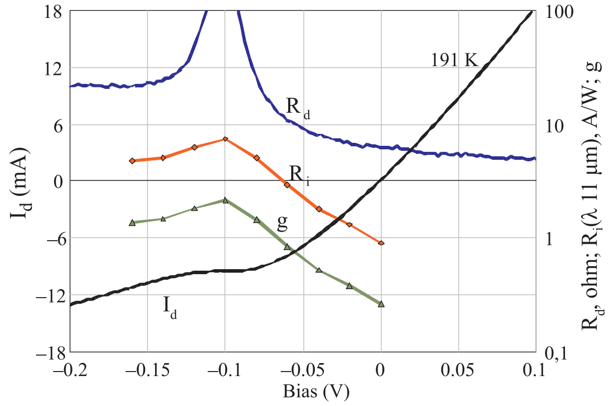

Fig.14. The dark current I_d, the dynamic resistance R_d, the current responsivity R_i, $\lambda = 11$ μm, and photoelectric gain g *vs*. bias at 191 K.

The size analysis has revealed bulk origin of the dark currents at any reverse voltages. The measured dark current is much greater than might be expected from simulations. This indicates large Shockley-Read generation or a major deviation of real device architecture from the theoretical design. The last reason seems to be more probable in view of SIMS measurements (Fig. 15) that revealed unexpected too large iodyne doping at the N^+/absorber interface and adjacent part of the absorber region.

The measured spectral response of the device is close to expectations. Significant photoelectric gain (Fig. 14) is observed for reverse bias corresponding to the peak of dynamic resistance. The shot noise limited spectral detectivity is shown in Fig. 16 for unbiased and biased device. The biased device exhibits remarkable performance at $\lambda = 11$ μm, 14 μm, and 16 μm. Unfortunately, reverse biased diodes show significant low frequency noise with ~10 MHz knee frequency resulting in significant reduction of performance in the required operational bandwidth of 100 kHz to 2MHz range. As the 1/*f* noise is usually proportional to the dark current [64], the refinement of real detector architecture should move the 1/*f* noise knee to low frequencies.

The measured cut-on wavelength of the prototype devices was larger (~2.8 μm) than required. The problem was due to less efficient iodyne doping of wide gap material.

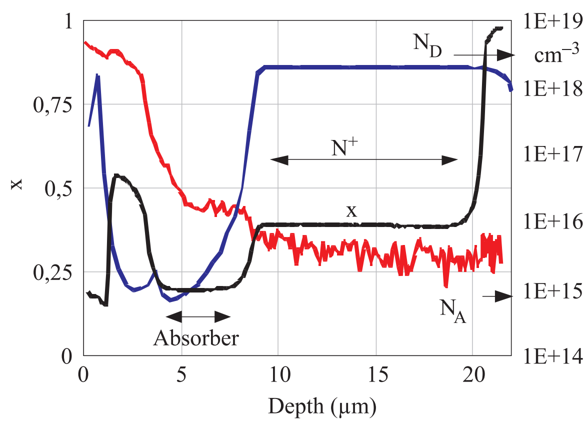

Fig. 15. Composition, iodine and arsenic profiles measured with SIMS.

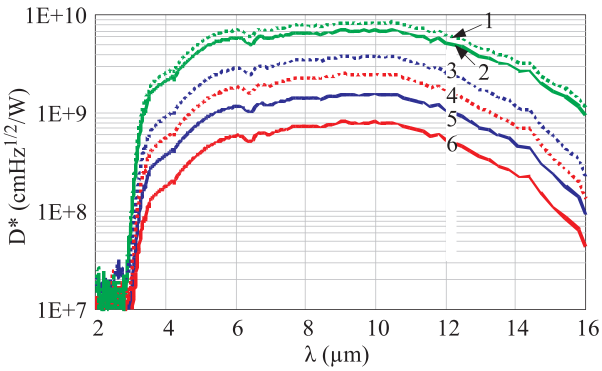

Fig.16. Measured shot noise limited D^* *vs*. λ of detector itself and predicted D^* of the detection module at 191 K and f ~10 MHz for 0 V, smaller and greater reverse bias: 1 – 0.16 V, D^* detector noise only, 2 – 0.16 V, detector and PA noise, 3 – 0.03 V, detector noise only, 4 – 0 V, detector noise only, 5 – 0.03 V, detector and PA noise, 6 – 0 V, detector and PA noise.

The improved growth procedure have made possible to grow N^+ layers with < 50% absorption at wavelength as short as 1.7 μm.

Summarizing, the numerical simulations show promise for high performance detection of IR radiation within the required spectral range with the use of optically immersed photodiodes operating with 4-stage Peltier cooling.

Prototype structures were made and characterized. It seems that their parameters are limited by faults in their architecture that differs from that determined by simulation.

Further work will be aimed at minimizing dark current and thus 1/f noise by refinement of MOCVD growth.

4. Conclusions

The development of $Hg_{1-x}Cd_xTe$ in Poland began with academic research and resulted in industrial exploitation of the material for infrared photodetectors. Polish efforts have been concentrated mostly on the uncooled long wavelength devices rather than on the mainstream of detector industry-the LN-cooled 2D arrays for thermal imaging. That has happened mostly due to the lack of adequate financing, the near room temperature devices did not require extreme technologies and expensive equipment.

Ways to perfect detection without cooling have been recognized and suitable technologies developed. The HOT devices corresponding to 3D heterostructure concept have been implemented with ISOVPE and MOCVD epitaxial techniques and specific processing technologies. That became the basis of fast cycle times and flexible low volume manufacturing of the infrared detectors with affordable costs corresponding to the niche needs of the IR industry.

Acknowledgements

We would like to thank FP7 MEMFIS project for partly sponsoring this research.

References

1. W.D. Lawson, S. Nielsen, E.H. Putley, and A.S. Young, "Preparation and properties of HgTe-CdTe", *J. Phys. Chem. Solids* **9**, 325–329 (1959).
2. R.R. Galazka and W. Giriat, "Electrical properties of the CdTe-HgTe system", *Bull. Acad. Polon. Sci.* **9**, 281 (1961).
3. R. Gałązka, "Preparation, doping and electrical properties of $Hg_{0.9}Cd_{0.1}Te$", *Acta Phys. Polon.* **24**, 791–800 (1963).
4. W. Giriat, Z. Dziuba, R.R. Galazka, L. Sosnowski, and T. Zakrzewski, "Electrical properties of the semiconducting system Cd_xHg_{1-x} Te", *Proc. 7^th ICPS*, Dunod Editeur, Paris, 251 (1964).
5. W. Giriat and M. Grynberg, "Photoelectromagnetic infrared detector", *Przegląd Elektroniki* **4**, 216–221 (1963). (in Polish)
6. J. Piotrowski and A. Rogalski, *Semiconductor Infrared Detectors*, WNT Warsaw, 1984. (in Polish)
7. G. Cohen-Solal and Y. Marfaing, "Transport of photocarriers in $Cd_xHg_{1-x}Te$ graded-gap structures", *Solid. State Electron.* **11**, 1131–1147 (1968).
8. J. Piotrowski, "A new method of obtaining $Cd_xHg_{1-x}Te$ thin films", *Electr. Technol.* **5**, 87–89 (1972).
9. J. Piotrowski, "Electrical and photoelectric properties of $Hg_{1-x}Cd_xTe$ films", *Msc Dissertation*, MUT, Warsaw, 1973. (in Polish)
10. E. Igras, R. Jeżykowski, T. Persak, J. Piotrowski, and Z. Nowak, "Epitaxial $Cd_xHg_{1-x}Te$ layers as infrared detectors", *Proc. 6^th Int. Symp. on Photon Detectors*, Siofok, Hungary, 221-236 (1974).
11. J. Piotrowski, W. Galus, and M. Grudzień, "Near room-temperature IR photo-detectors", *Infrared Phys.* **31**, 1–48 (1991).
12. Z. Nowak, J. Piotrowski, and J. Rutkowski, "Growth of HgZnTe by cast-recrystallization", *J. Cryst. Growth* **89**, 237–241 (1988).
13. K. Adamiec, A. Maciak, Z. Nowak, and J. Piotrowski, "ZnHgTe as a material for ambient temperature 10.6 micrometer photodetectors", *Appl. Phys. Lett.* **54**, 143-144 (1989).
14. J. Piotrowski, K. Adamiec, and A. Maciak, "High-temperature 10.6-μm HgZnTe photodetectors", *Infrared Phys.* **29**, 267–270 (1989).
15. P. Brogowski, H. Mucha, and J Piotrowski, "Modification of mercury cadmium telluride, mercury manganese tellurium, and mercury zinc telluride by ion etching", *Phys. Stat. Sol.*, **114** (a), K37 (1989).
16. P. Brogowski and J. Piotrowski, "The *p*-to-*n* conversion of HgCdTe, HgZnTe and HgMnTe by anodic oxidation and subsequent heat treatment", *Semicond. Sci.* **5**, 530–532 (1990).
17. E. Igras and J. Piotrowski, "A new (Cd,Hg)Te photodiode type with protected junction surface", *Opt. Appl.* **6**, 99-106 (1976).
18. A. Rogalski, J. Piotrowski, and J. Gronkowski, "A modified hot wall epitaxy technique for the growth of CdTe and $Hg_{1-x}Cd_xTe$ epitaxial layers", *Thin Solid Films* **191**, 239– 245 (1990).
19. L. Kubiak, P. Madejczyk, J. Wenus, W. Gawron, K. Jóźwikowski, J. Rutkowski, and A. Rogalski, "Status of HgCdTe photodiodes at the Military University of Technology", *Opto--Electron. Rev.* **11**, 211–226 (2003).
20. A. Rogalski and J. Piotrowski, "Intrinsic infrared photodetectors", *Prog. Quant. Electron.* **12**, 87–289 (1988). Pergamon Press.
21. J. Piotrowski, A. Jóźwikowska, K. Jóźwikowski, and R. Ciupa, "Numerical analysis of longwavelength extracted photodiodes", *Infrared Phys.* **34**, 565–572 (1993).

22. *Infrared Photon Detectors*, edited by A. Rogalski, SPIE Optical Engineering Press, Bellingham, Washington USA, 1995.
23. A. Rogalski, *Infrared Detectors*, Gordon and Breach Science Publishers, Amsterdam, 2000.
24. A. Rogalski, K. Adamiec, and J. Rutkowski, *Narrow-gap Semiconductor Photodiodes*, SPIE Press, Bellingham, 2000.
25. A. Rogalski, "Hg-based alternatives to MCT", chapter in *Infrared Detectors and Emitters: Materials and Devices*, pp. 377–400, edited by P. Capper and C.T. Elliott, Kluwer Academic Publishers, Boston, 2001.
26. A. Rogalski, "Infrared detectors: status and trends", *Prog. Quant. Electron.* **27**, 59–210 (2003).
27. A. Rogalski, "Photon detectors", chapter in *Encyclopedia of Optical Engineering*, pp. 1985–2035, edited by R. Driggers, Marcel Dekker, Inc., New York, 2003.
28. A. Rogalski, *Infrared Detectors: Developments*, SPIE Milestone Series, SPIE Optical Engineering Press, Bellingham, Washington USA, 2004.
29. A. Rogalski, "HgCdTe infrared detector material: history, status and outlook", *Rep. Prog. Phys.* **68**, 2267–2336 (2005).
30. P. Becla, E. Dudziak, and J.M. Pawlikowski, "Spectral sensivity of the photovoltaic effect in $Cd_xHg_{1-x}Te$ *p-n* junctions", *Opt. Appl.* **4**, 3–5 (1974).
31. J.M. Pawlikowski and P. Becla, "Some properties of photovoltaic $Hg_{1-x}Cd_xTe$ detectors for infrared radiation", *Infrared Phys.* **15**, 331–337 (1975).
32. P. Becla and J.M. Pawlikowski, "Epitaxial $Hg_{1-x}Cd_xTe$ photovoltaic detectors", *Infrared Phys.* **16**, 457–464 (1975).
33. J.M. Pawlikowski, "Photoconductivity of graded-gap $Hg_{1-x}Cd_xTe$", *Infrared Phys.* **19**, 179–184 (1978).
34. J.M. Pawlikowski, "Application of epitaxial graded-gap semiconductor layers broad range photodetectors", *Thin Solid Film* **50**, 269–272 (1978).
35. P. Becla and E. Placzek-Popko, "Electrical properties of infrared photovoltaic $Hg_{1-x}Cd_xTe$ detectors", *Infrared Phys.* **21**, 323–332 (1981).
36. M. Nowak, "The photomagnetoelectric effect and photoconductivity for non-normal incidence of radiation", *Phys. Stat. Sol. (a)* **80**, 691–701 (1983).
37. M. Grudzień and J. Piotrowski, "Monolithic optically immersed HgCdTe IR detectors", *Infrared Phys.* **29**, 251–253 (1989).
38. J. Piotrowski, W. Galus, and M. Grudzień, "Near room-temperature IR photo-detectors", *Infrared Phys.* **31**, 1–48 (1991).
39. J. Piotrowski, W. Gawron, and Z. Djuric, "New generation of near-room-temperature photodetectors", *Opt. Eng.* **33**, 1413 –1421 (1994).
40. J. Piotrowski, "$Hg_{1-x}Cd_xTe$ infrared photodetectors", in *Infrared Photon Detectors*, pp. 391–494, edited by A. Rogalski, SPIE, Bellingham, 1995.
41. J. Piotrowski and W. Gawron, "Ultimate performance of infrared photodetectors and figure of merit of detector material", *Infrared Phys. Techn.* **38**, 63–68 (1997).
42. J. Piotrowski and M. Razeghi, "Improved performance of IR photodetectors with 3D gap engineering", *Proc. SPIE* **2397**, 180–192 (1995).
43. J. Piotrowski, M. Grudzień, Z. Nowak, Z. Orman, J. Pawluczyk, M. Romanis, and W. Gawron, "Uncooled photovoltaic $Hg_{1-x}Cd_xTe$ LWIR detectors", *Proc. SPIE* **4130**, 175– 184 (2000).
44. J. Piotrowski, "Uncooled operation of IR photodetectors", *Opto-Electron. Rev*. **12**, 11–122 (2004).
45. J. Piotrowski and A. Rogalski, *High-Operating-Temperature Infrared Photodetectors*, SPIE, Bellingham (2007).
46. A. Piotrowski and J. Piotrowski, *Room Temperature Photodetectors*, Willey (to be published in 2009).
47. J. Piotrowski, Z. Djurić, W. Galus, V. Jović, M. Grudzień, Z. Djinović, and Z. Nowak, "Composition and thickness control of $Cd_xHg_{1-x}Te$ layers grown by open tube isothermal vapour phase epitaxy", *J. Cryst. Growth* **83**, 122–126 (1987).
48. J. Piotrowski, Z. Nowak, M. Grudzień, W. Galus, K. Adamiec, Z. Djurić, V. Jović, and Z. Djinović, "High capability, quasi closed growth system for isothermal vapour phase epitaxy of (Hg,Cd)Te", *Thin Solid Film* **161**, 157–169 (1988).
49. Z. Djuric and J. Piotrowski, "Generalized model of the isothermal vapour phase epitaxy of HgCdTe", *Appl. Phys. Lett*. **51**, 1699–1701 (1987).
50. K. Adamiec, M. Grudzień, Z. Nowak, J. Pawluczyk, J. Piotrowski, J. Antoszewski, J. Dell, C. Musca, and L. Faraone, "Isothermal vapour phase epitaxy as a versatile technology for infrared photodetectors", *Proc. SPIE* **2999**, 34–43 (1997).
51. A. Piotrowski, P. Madejczyk, W. Gawron, K. Klos, M. Romanis, M. Grudzień, A. Rogalski, and J. Piotrowski, "MOCVD growth of $Hg_{1-x}Cd_xTe$ heterostructures for uncooled infrared photodetectors", *Opto-Electron. Rev.* **12**, 453–458 (2004).
52. A. Piotrowski, P. Madejczyk, W. Gawron, K. Kłos, J. Pawluczyk, M. Grudzień, J. Piotrowski, and A. Rogalski, "Recent progress in MOCVD growth of $Hg_{1-x}Cd_xTe$ heterostructures for uncooled infrared photodetectors", *Proc. SPIE* **5957**, 273–284 (2005).
53. A. Piotrowski, W. Gawron, K. Klos, J. Pawluczyk, J. Piotrowski, P. Madejczyk, and A. Rogalski, "Improvements in MOCVD growth of $Hg_{1-x}Cd_xTe$ heterostructures for uncooled infrared photodetectors", *Proc. SPIE* **5957**, 108–116 (2005).
54. A. Piotrowski, P. Madejczyk, W. Gawron, K. Kłos J. Pawluczyk, J. Rutkowski, J. Piotrowski, and A. Rogalski, "Progress in MOCVD growth of HgCdTe heterostructures for uncooled infrared photodetectors", *Infrared Phys. Techn.* **49**, 173–182 (2007).
55. Vigo System S.A. (2008, unpublished)
56. VIGO System S.A. Website http://www.vigo.com.pl
57. A. Piotrowski, K. Kłos, W. Gawron, J. Pawluczyk, Z. Orman, and J. Piotrowski, "Uncooled or minimally cooled 10 μm photodetectors with subnanosecond response time", *Proc. SPIE* **6542**, 65421B (2007).
58. A. Bocci, A. Drago A. Marcelli, and J. Piotrowski, "Beam diagnostics at IR wavelengths at NSRL", *09 Particle Accelerator Conference*, Vancouver. (to be published).
59. MEMFIS project website, http://www.memfis-project.eu/
60. T. Elliott, N.T. Gordon, and A.M. White, "Towards background-limited, room-temperature, infrared photon detectors in the 3–13 μm wavelength range", *Appl. Phys. Lett.* **74**, 2881–2883 (1999).
61. M.A. Kinch, *Infrared Detector Materials*, SPIE Press, Bellingham, 2007.
62. APSYS Device Simulator, Software Package, Crosslight Software Inc, Canada.
63. C.T. Elliott, "Photoconductive and non-equilibrium devices in HgCdTe and related alloys", in *Infrared Detectors and Emitters: Materials and Devices*, pp. 279–312, edited by P. Capper and C.T. Elliott, Kluwer Academic Publishers, Boston, 2000.
64. M.K. Ashby, N.T. Gordon, C.T. Elliott, C.L. Jones, C.D. Maxey, L. Hipwood, and R. Catchpole, "Investigation into the source of 1/*f* noise in $Hg_{1-x}Cd_xTe$ diodes", *J. Electron. Mater.* **33**, 757–765 (2004).